Preparatory investigations for the construction of a table-top PMD station

Bachelorarbeit aus der Physik

Vorgelegt von
Franziska Leitl
30.01.2019

Erlangen Centre for Astroparticle Physics
Friedrich-Alexander-Universität Erlangen-Nürnberg

Betreuer: Prof. Dr. Christopher van Eldik

Abstract

Phase Measuring Deflectometry is a well known deflectometric technique to measure reflecting free forms which has successfully been used in the past to measure mirror facets of CTA telescopes. For this method a known pattern is projected onto the mirror surface. The distortion of this pattern due to the reflection on the surface is measured by cameras and the evaluation of the images provides information about the surface of the mirror.
The goal of the following thesis is to study the properties of a planned table-top Phase Measuring Deflectometry station with the use of simulations. The results of the table-top setup can also be transferred to the full-sized mirror measurement station because of their similar design.
For this purpose, a possible design for a table-top measuring station was derived and simulated. These simulations were repeated to study the effects of different camera placements and resolution changes of the cameras and the screen on the mirror measurement capability. It can be shown that it is possible to move the cameras within certain limits in the centimeter range from their original position without impacting the measurement results too much. It can also be shown that the results heavily depend on the choice of the camera and screen resolution. The general trend is that a higher screen resolution can accomplish better results but the camera resolution has to be adjusted accordingly. Finally, it is shown that measurement results worsen heavily in the presence of unknown displacements and misalignments of a single camera. Tilting a camera in the order of 0.001 degree or shifting it in the order of 100 µm can already lead to deviations of almost 30 percent. Shifts in the millimeter range can even cause deviations of about 700 percent.

Contents

1 Introduction to gamma-ray astronomy and the CTA project

The earth is hit by particles originating from outer space on a daily basis. This was discovered by the Austrian physicist Victor Hess in 1912. He measured the ionization rate of the atmosphere with a hot air balloon and detected that the rate increased with a rising altitude. This marked the birth of astroparticle physics. Nowadays, it is known that those particles, also known as cosmic rays, consist of many different kinds of particles, both charged and uncharged. When the primary radiation hits the terrestrial atmosphere, secondary radiation is generated by the collision of the primary radiation with the nuclei of the atmosphere. These secondary particles then reach the ground as a particle shower [3].
The origin of these primary cosmic rays is of interest. But, since charged particles are deflected by magnetic fields on their way to earth, their origin cannot be determined. For uncharged particles, such as gamma rays, this is not an issue. Therefore they are a useful tool to analyze the origin of cosmic particle accelerators.

One way to observe gamma rays coming from out of space would be through satellites like, for example, the Fermi Large Area Telescope (LAT). However, since the particle flux of cosmic rays decreases with increasing particle energy, a large area is required for the sufficient investigation of high-energy gamma rays. This is not practicable for satellites as the costs for their construction would be too high. Therefore other possibilities have to be explored in order to be able to investigate very-high-energy radiation.
In recent years, numerous discoveries in the field of astroparticle physics have been made with the help of ground-based Cherenkov Telescopes. When gamma rays interact with the atmosphere, electrons, positrons and photons are generated. If the velocity of the charged secondary particles in matter is higher than the phase velocity of electromagnetic waves in the same medium, a blue light is emitted towards the ground in a conical shape. This light is also called Cherenkov light and can be measured by ground-based telescopes with big mirror surfaces. The incoming light is reflected by the mirrors and then focused into a camera that is mounted to the telescope and consists of photomultipliers [2]. The print that is left over in the camera image can be read out and holds information about the energy and direction of the primary particle (see figure 1). Ground-based telescope arrays are able to cover a much larger area than satellites which makes the detection of gamma rays in much higher energy ranges possible.
Currently a new cluster of ground-based telescopes is in the works which is called Cherenkov Telescope Array (CTA). They are aiming to surpass any existing ground-based Cherenkov telescope by far with a sensitivity that is orders of magnitude higher than what has been built before. Additionally, it will provide a full-sky view through telescope arrays that are located in the northern and southern hemisphere. The energy of detectable gamma rays will lie between a few tens of GeV and several 100s of TeV [1].

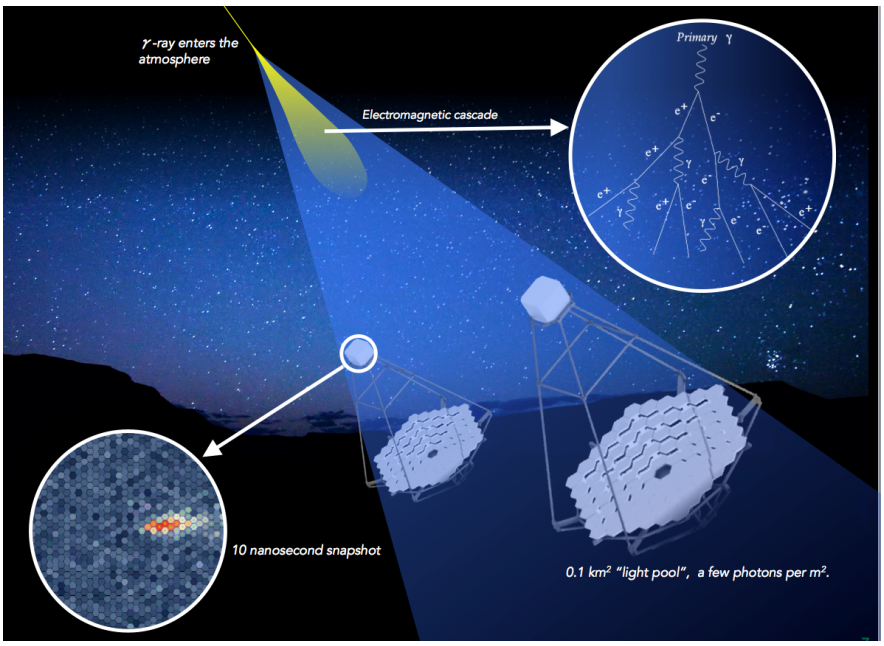

Figure 1: Gamma-ray detection via CTA. The incoming gamma rays cause Cherenkov light which gets focused into the camera of the telescopes. The leftover print can be read out afterwards (image from [4]).

To obtain this energy range, three different types of telescope arrays are built. The first kind focuses on detecting gamma rays in the range below 100 GeV where the incoming flux of particles is high. Therefor large-size telescopes (LST) with a parabolic mirror and a diameter of 23 m are in the works. Mid-size telescopes (MST) are supposed to observe the main energy range from 0.1-10 TeV. Right now there are two prototypes to be considered for this job. The first is a spherical MST with Davies-Cotton reflector and a mirror diameter of 12 m. The second is a dual-mirror design with Schwarzschild-Couder optics that allows a much finer pixelation. For high-energy gamma rays above 10 TeV the particle flux is much lower. That is why a larger area covered with telescopes is needed to measure approximately the same number of particles compared to low-energy gamma rays. Currently it is planned to build a large number of small-size telescopes (SST) with around 5-8 m diameter as a scaled down version of the MSTs. Since the surface area of the aforementioned telescopes is very large, it is useful to use many small mirror facets instead of one big mirror because they are easier to obtain and a lot cheaper [2].

Because gamma-ray measurements depend strongly on the correct reflection of the incoming Cherenkov light, it is crucial to have well functioning mirrors. For that, they have to be tested thoroughly before they can be mounted to the telescopes. Hence, measuring the point spread function (PSF) of the mirrors is strictly necessary. It provides information about the reflection of a point-like light source that reaches a reflective surface from a certain distance. The size of the PSF can be evaluated with the help of the d80. It is the diameter of the circle that includes 80 percent of the reflected light. The CTA mirror facets can only be used if the

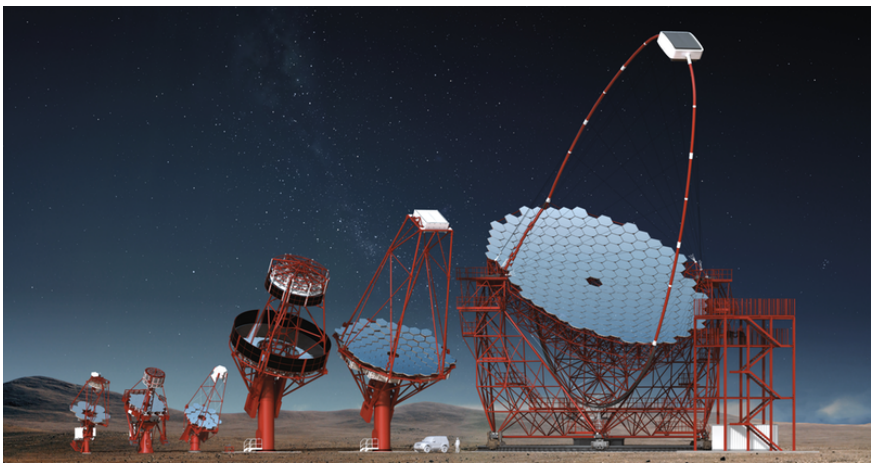

Figure 2: From the left: Three different SST prototype designs, two MST prototype designs and the LST prototype design (image from [5]).

d80 is smaller than $\frac{2}{3}$ of the diameter of the pixel size of the camera mounted to the telescope [7].
Nowadays CTA mirror facets are measured via a method called Phase Measuring Deflectometry (PMD). Setups that apply this measuring technique are already in use. In order to be able to examine the systematics of these setups even further, now a table-top version of the construction is planned, so that investigations can continue without using the structure that is already used for measurements. Since the small setup will correspond approximately to the large one, information regarding the systematics of the setup could be transferred to the large version without having to interrupt measurements or delay them due to necessary recalibrations.

The goal of this thesis is to design such a table-top Phase Measuring Deflectometry station and study its properties with the use of simulations.
First, the basic procedure for measuring mirrors with the PMD method is presented. This includes the measurement technique in itself and the setup that is currently used to measure MST mirror facets. Since the final design of the table-top station is a simulation, the general procedure of simulating the setup will also be explained. Afterwards, the design for the table-top setup will be introduced and analyzed. First the properties of the designed construction are shown, then parts of the setup are systematically changed in order to find possible limits or improvements for the analysis with this setup. In the end the design is tested in regard to externally induced changes.

2 The basics of Phase Measuring Deflectometry

The following chapter describes the general principle of Phase Measuring Deflectometry. First the basic means necessary for the PMD measurement are described. Then the structure of the setup used for CTA mirrors is presented. Lastly, in regard to the fact that the table-top setup will only be simulated in this thesis, it is discussed how these simulations are developed and what is necessary in order to obtain the data for the evaluation of the mirror.

2.1 The principle of PMD

The general idea of Phase Measuring Deflectometry is to measure the quality of specular surfaces by observing their reflections. For this purpose, a screen showing a known pattern is placed in a way that its reflection can be observed by a camera within the aforementioned surface. A picture of this reflection taken by the camera can then be used to identify the curvature of the tested mirror surface. It will later be used to determine whether or not the mirror fulfills necessary quality requirements.

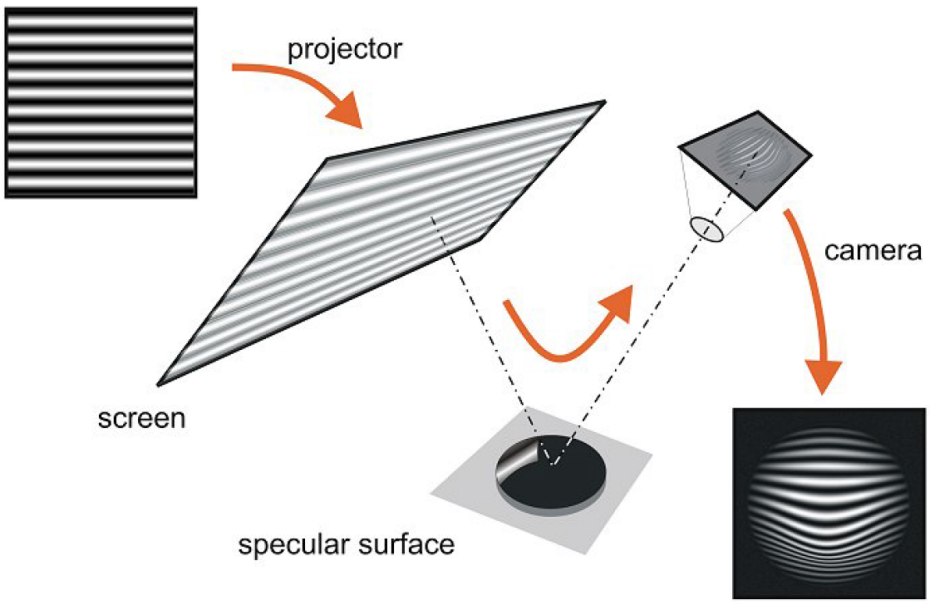

Figure 3: Schematic view of a PMD measurement. The screen projects a sinusoidal pattern onto the reflective surface. The camera takes pictures of the distortion to identify the curvature of the examined object (image from [9]).

The light rays must be tracked from the screen to the camera, so that each camera pixel has an assigned screen pixel. To find out which screen pixel is projected onto the corresponding camera pixel, the pattern that is used for the measurement must be unique for every screen pixel. The approved method is to use two coprime sinusoidal distributed intensity functions and shift their phases repeatedly in x- and y-direction on the screen. This prevents that different pixels on the screen

resemble each other. Lastly, one has to evaluate the intensity distribution of the resulting camera pictures to connect the pixels of the camera to the corresponding pixels of the screen.
The radius of curvature of a mirror can then be identified through its surface normals. The incoming light gets reflected off of the mirror with an angle of reflection equal to its angle of incidence. When given the exact positions of the mirror, the screen and the camera, one can compute the surface normals of the mirror and therefore easily calculate its radius of curvature using geometric deliberations [9].

The position of the screen and camera is usually known but the one of the specular surface is not. This leads to a spatial ambiguity of the mirror (see figure 4). Technically, spatial ambiguities can be solved by using a stereo setup of multiple cameras. In case of mirror measurements, this is not possible due to the geometry of the setup since the mirror is lacking necessary fixed points. Instead the ideal model of the examined mirror is chosen as an alternative. Its surface description is used to find the best fitting mirror location and radius. For this, the position and radius of the ideal mirror is varied as the other objects stay fixed. In the end the best-fit location of the ideal mirror with the least deviations from the real measurement is chosen as real mirror position [7].

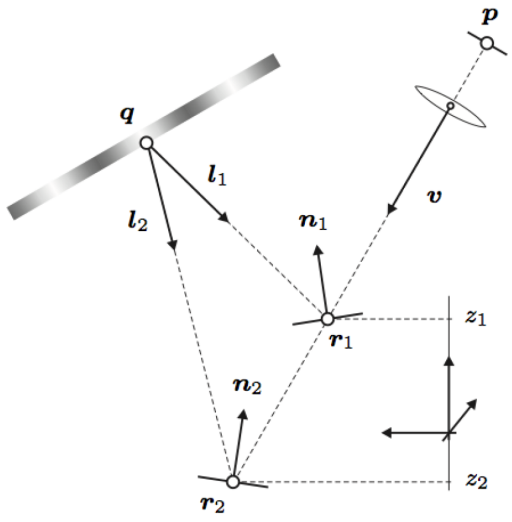

Figure 4: Spatial ambiguity of specular surface. Point q is reflected into point p despite of two different mirror positions (here r_1, n_1 and r_2, n_2) (image from [6]).

After the PMD evaluation, the position and curvature of the mirror can be evaluated. Then the d80 of the mirror has to be found to evaluate the quality of the mirror. For that, the $2f$ method is used. It works as follows: a point-like light source and a camera are placed in a distance of two focal lengths from the mirror surface. The light of the source will be reflected in the mirror and is then focused into the camera. With that approach, the PSF and d80 can be determined by ray-tracing [9].

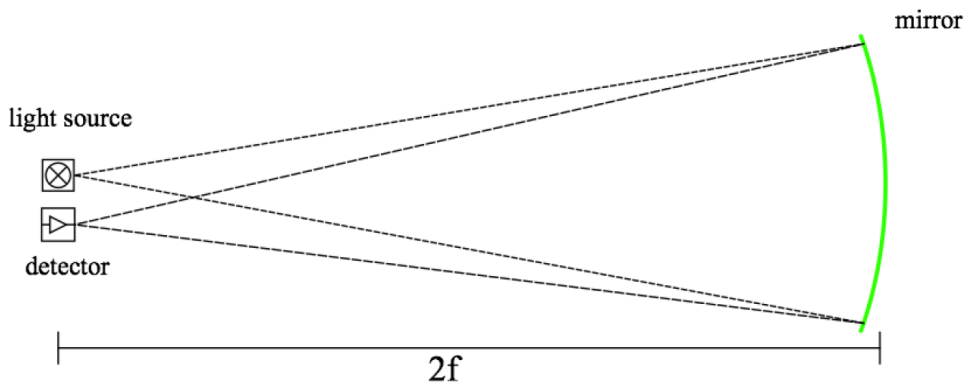

Figure 5: Schematics for obtaining the PSF of a mirror with the help of the $2f$ method (image from [6]).

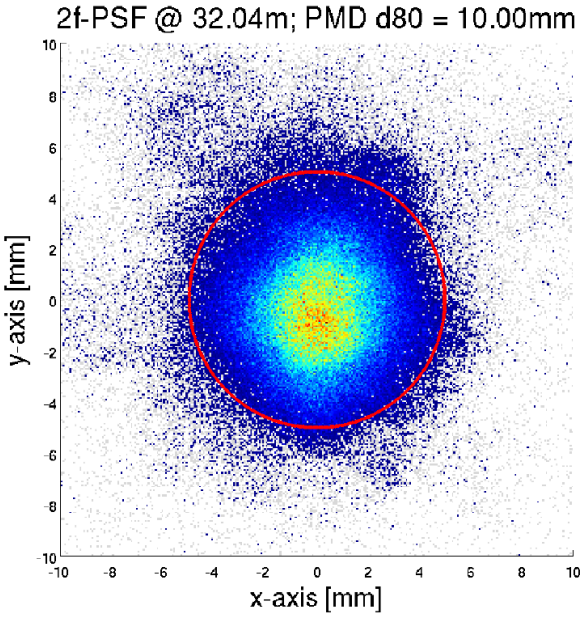

Figure 6: Example PSF results of a spherical mirror (image from [6]).

2.2 The measurement setup

The design of the table-top setup for PMD measurements, which will be presented in the next chapter, is based on the model of a full-size PMD measuring station for CTA mirror facets like, for example, the MST mirror facets. One way to measure those mirror facets is to use a Short Working Distance setup (SWD). It is a relatively compact setup which can fit comfortably into a room (see figure 7). Compared to Long Working Distance setups (LWD), which at least require a measuring space of the radius of curvature of the measured mirror facet, the SWD setup saves a lot of working space. The MST mirror facets have a radius of curvature of 32 m, so using a LWD setup for the measurement would require a long hall [6].

As mentioned before, a screen, a mirror and at least one camera is required for PMD measurements. However, more than one camera is needed if the mirror surface cannot be covered with just one camera. In the case of MST mirrors, four cameras are used. They are mounted to a framework that enables each camera to cover a corner of the mirror facet with a small overlap of the adjacent pictures. The four different pictures can then be merged together for the evaluation since the positions and orientations of each camera are known. This way no data will be lost by cutting of mirror areas.
In addition to saving work space, the SWD setup also allows a flexible placement of the measured mirror as the complete coverage of the mirror by the cameras is the only criterion that has to be guarantied [6]. Figure 7 shows a SWD setup for a PMD measurement of MST mirror facets that was built in Erlangen.

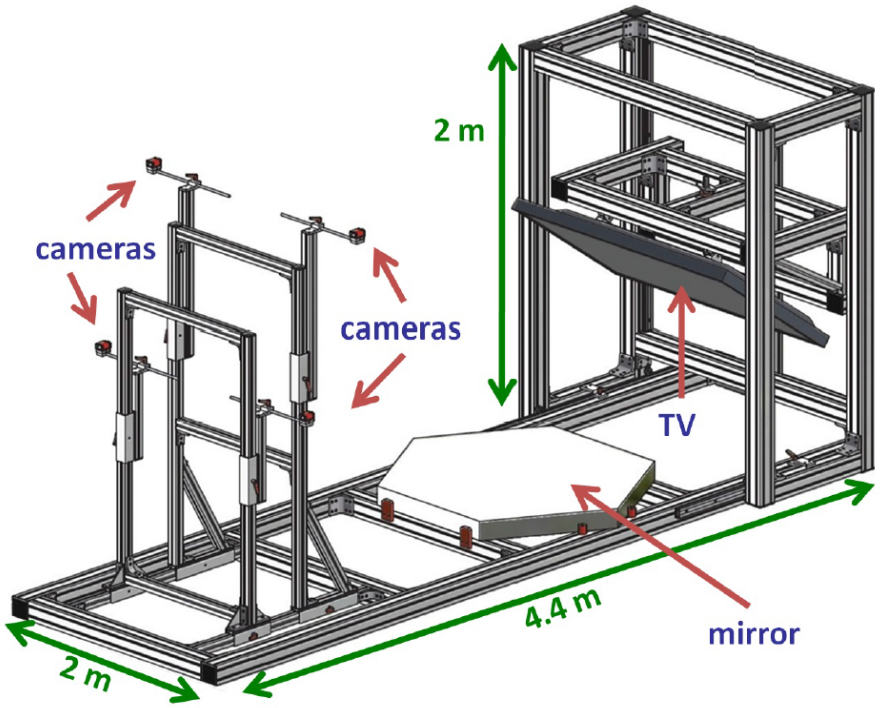

Figure 7: Example of a Short Working Distance PMD measurement setup (image from [9]).

2.3 Simulating the setup

In measurements the images of the mirror are taken by a camera which shows the distorted pictures of the reflected pattern but, because the table-top setup will only be simulated, no real pictures can be taken.
The simulation itself was created by a specialized ray-tracing program called Mitsuba [8]. Not only is it able to track light rays coming from different light sources in a 3D setting despite various intersections with other obstacles, it is

furthermore able to render pictures of these so called scenes coming from different perspectives. In the case of the PMD setup the scenes consist of a mirror, four cameras and the screen projection which acts as the only light source in the scene. The images for each respective camera are rendered by tracing back the light rays from the cameras to the screen.

The screen pattern itself is created by using two coprime sinusoidal intensity distributions which are superimposed on each other to prevent a pattern which is repeating itself every 2π. Therefor the chosen stretch factors, which determine the frequency of the pattern on the screen, were 7 for one distribution and 8 for the other. To get the best possible end results, it is wise to repeat the measurement with another set of stretch factors and combine the results of the two measuring series.
The other stretch factors used in this experiment were 7×24 and 8×24 which were the ideal stretch factors for the SWD setup in Erlangen. For each stretch factor 8 different images were taken in total by phase shifting the pattern 4 times in x- and y-direction respectively.
Those pictures will then be used to calculate the local slope which ultimately sheds light on the 3D information of the mirror and its PSF.

3 The table-top design

The following describes the properties of the table-top setup and its results obtained with the PMD and PSF measurements. In general, the design resembles the big setup with which one measures CTA mirror facets, but it is constrained to a size that can fit on a regular laboratory table. In addition, in contrast to the large setup, the complete surface of the examined mirror can be surveyed with each camera individually due to its small size. In the following the exact parameters that are used in the simulation for the reference setup are given because even small changes of the parameters of the mirror, the cameras and the screen will lead to slightly different measurement results.
The mirror used in the following tests has a circular form with a diameter of 20 cm and its radius of curvature equals 30 m. This results in a height of the reflective mirror surface of $h = 0.1666671297\,\text{mm}$.

Figure 8: On the left, a simulation of a camera shot of the large setup is shown where the complete mirror cannot be covered by a single camera (image from [6]). On the right, a simulation of a camera shot of the table-top setup is shown where the complete coverage is possible.

As seen in the model of the normal-sized SWD setup in figure 7, the four cameras are positioned in two camera rows with the upper left and upper right camera, camera 0 and camera 1, forming the upper camera row and the lower left and lower right camera, cameras 2 and 3, forming the lower row when looking towards the mirror. All cameras have a resolution of 1280×960, a pixel size of $3.75\,\mu\text{m}$ and a focal length of 16 mm. The screen has an angle of about 80 degree to the surface plane of the mirror. It is 60 cm wide, has an aspect ratio of 16:9 with a resolution of 1920×1080 and a pixel size of $312.5\,\mu\text{m}$ in the simulation.
Table 1 will present the coordinates and orientations of the screen and the four cameras used in this setup in global coordinates. The global coordinate system describes the shared coordinate system of all objects. The zerobase specifies the x-, y- and z-coordinates of the respective objects in the global coordinate system and therefore their position in the 3D space while the xbase and ybase vectors describe the x- and y-base vectors of each individual object in global coordinates and therefore determine the orientation of each object in the 3D space. When looking from the cameras towards the screen, the x-axis of the global coordinate system points to the right, the y-axis points from the cameras to the screen and the z-axis points upwards.

The mirror is placed 10 cm elevated from the origin of the global coordinate system in z-direction. Like in the model, the setup is symmetrical.

Screen	
zerobase	(0 | 0.18 | 0.34)
xbase	(1 | 0 | 0)
ybase	(0 | -0.17364818 | 0.98480775)
Camera 0	
zerobase	(-0.2 | -0.53 | 0.8)
xbase	(0.97537065 | -0.13218365 | 0.1765774)
ybase	(0.2205722 | 0.58451632 | -0.78082557)
Camera 1	
zerobase	(0.2 | -0.53 | 0.8)
xbase	(0.97537065 | 0.13218365 | -0.1765774)
ybase	(-0.2205722 | 0.58451632 | -0.78082557)
Camera 2	
zerobase	(-0.3 | -0.58 | 0.6)
xbase	(0.93198532 | -0.2739963 | 0.23733813)
ybase	(0.36249601 | 0.70445058 | -0.61020162)
Camera 3	
zerobase	(0.3 | -0.58 | 0.6)
xbase	(0.93198532 | 0.2739963 | -0.23733813)
ybase	(-0.36249601 | 0.70445058 | -0.61020162)

Table 1: Coordinates and directional vectors of the screen and all cameras used for the table-top setup in global coordinates. All coordinates are measured in meters.

After having created the simulation setup, the PSF of the mirror can be measured with the approach presented in chapter 2. The shape of the PSF is almost circular and its d80 equals 0.65994 mm as seen in figure 9. The d80 increases with a rising distance from its supposed minimum. For small distances it seems like it increases in a more parabolic way and for bigger distances it seems like it rises almost linearly (see figure 10).
In general, one would expect the d80 of an ideal mirror, like the one used in this simulation, to correspond to 0. But this is obviously not the case. To achieve this result, a perfectly point-shaped light source would be necessary. In the simulation each individual screen pixel acts as a light source in the scene. Because the pixels are not perfectly point-shaped, but have an expansion, edge effects have to be taken into account. They lead to an expansion of the PSF and ultimately increase the d80. A perfect d80 can therefore not be achieved in this simulation.

The distance d_{min} at the point of minimal d80 in the $2f$ ray-tracing was fitted for a more accurate result since the user has only access to discrete slices with a distance of 20 mm (see figure 10). After the fit d_{min} equals 30002.05 mm. The radius of curvature r_{det} of the mirror equals 29.99648 m.

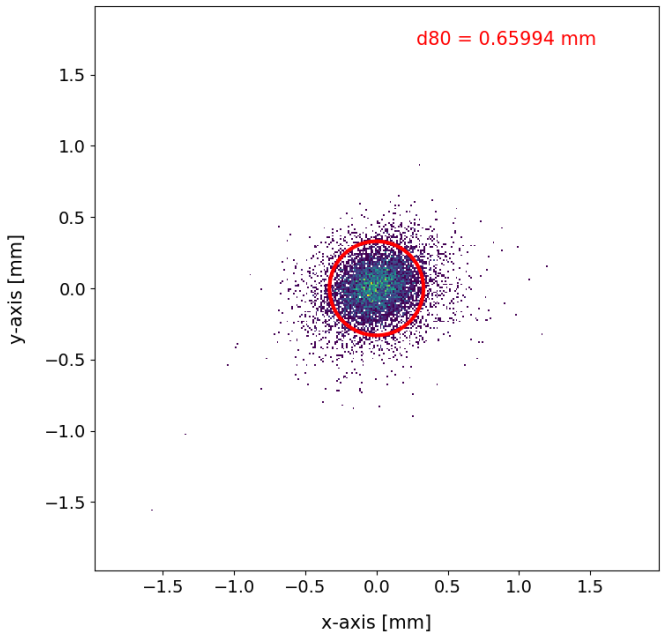

Figure 9: PSF of the mirror used for the table-top setup with the corresponding d80 marked in red.

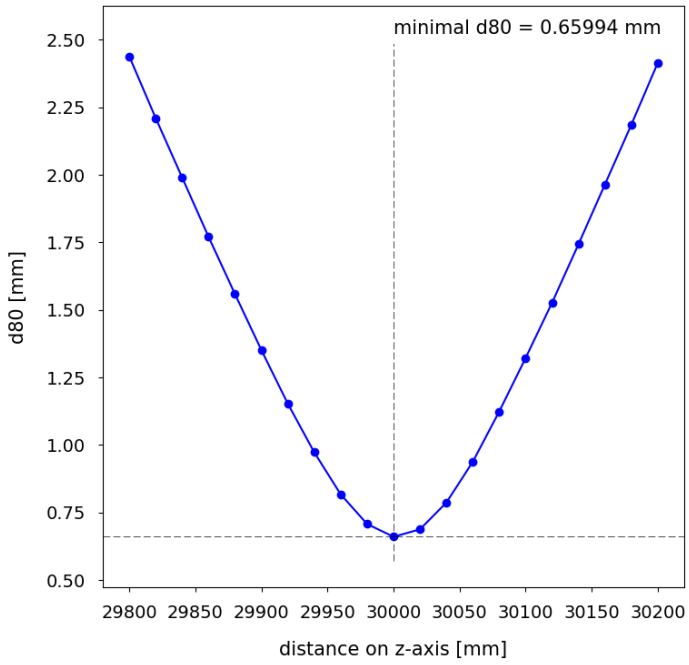

Figure 10: d80 as a function of the distance from the mirror in the $2f$ ray-tracing.

4 General analysis of the table-top setup

Now that the new setup is designed, it can be tested. At first, positional changes of the cameras were performed, starting with shifting only one camera at a time first and later shifting two cameras symmetrically to analyze the stability of the setup concerning the camera positions. Finally, different combinations of camera and screen resolutions were set in order to find out what influence they have on the test results and whether the reference setup can be improved by them.

4.1 Displacing one camera

The first changes where made by moving only one camera at a time. Through that the setup was made asymmetrical. The size of the shifts ranged from 1 nm to 10 cm which means several orders of magnitude were tested. The first camera that was moved was camera 0. Then displacements within the same range were performed for camera 3. Both cameras were moved towards the outer side of the table, changing their x-coordinates in the global coordinate system while making sure that the mirror surface still remained within the field of view of the shifted cameras. For that, a realignment of the camera orientations is necessary for a displacement of 10 cm.
The resulting r_{det} and d_{min} did not change much regardless of which camera has been shifted (see tables 2 and 3). The largest deviation for both values equals only 0.02 percent and none of the deviations follow a distinctive pattern.

shift in x [m]	r_{det} [m]	d_{min} for minimal d80 [mm]
$1 \cdot 10^{-1}$	29.99653	29999.32
$1 \cdot 10^{-2}$	29.99519	29998.42
$1 \cdot 10^{-3}$	29.99538	30000.52
$1 \cdot 10^{-4}$	29.99579	30000.02
$1 \cdot 10^{-5}$	29.99623	30002.80
$1 \cdot 10^{-6}$	29.99535	30001.78
$1 \cdot 10^{-9}$	29.99539	30000.23

Table 2: Measured r_{det} and d_{min} after shifting camera 0 in negative x-direction.

shift in x [m]	r_{det} [m]	d_{min} for minimal d80 [mm]
$1 \cdot 10^{-1}$	29.99682	29997.12
$1 \cdot 10^{-2}$	29.99505	29999.45
$1 \cdot 10^{-3}$	29.99405	30001.54
$1 \cdot 10^{-4}$	29.99586	30002.06
$1 \cdot 10^{-5}$	29.99743	30002.41
$1 \cdot 10^{-6}$	29.99403	29997.58
$1 \cdot 10^{-9}$	29.99429	30004.78

Table 3: Measured r_{det} and d_{min} after shifting camera 3 in positive x-direction.

Although the change of the d80 is small, it does reach deviations of up to 2.08 percent after shifting camera 0 and 3.47 percent after shifting camera 3. But, as seen for r_{det} and d_{min}, the deviations show no obvious behavior (see figure 11).

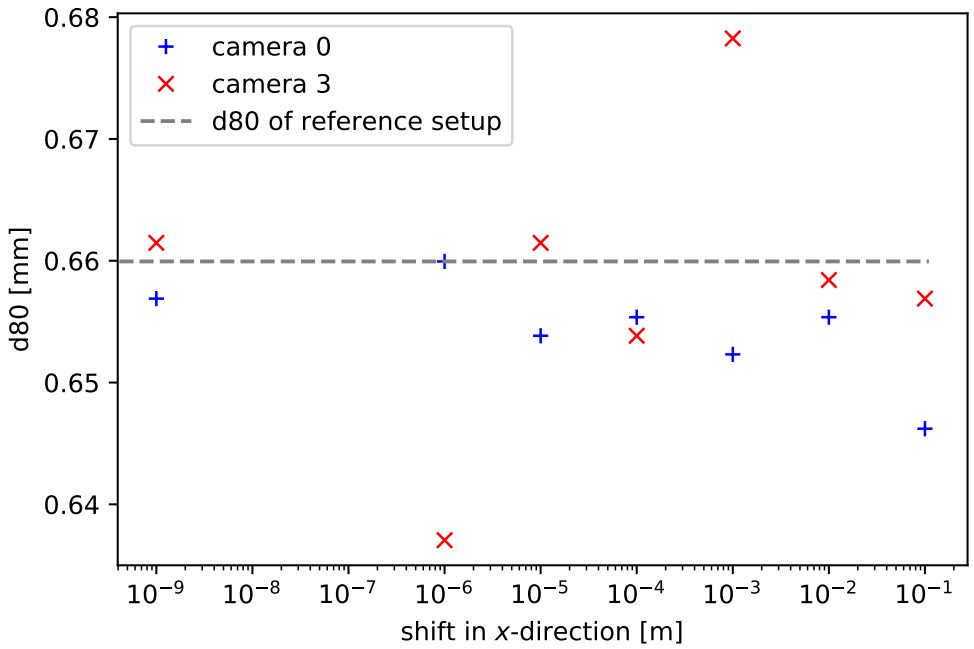

Figure 11: d80 measurement for separately shifted cameras 0 and 3 in x-direction.

Since r_{det} and d_{min} did not fluctuate much, although larger deviations occurred for the d80, it seems like these two values are quite stable in the simulation concerning the displacement of one camera in x-direction.
In general, it is also noticeable that the results after shifts of camera 0 and 3 in the range of 1 nm and 1 mm, which is small compared to the pixel size of the cameras, deviate about as much from the reference values as the results of shifts which are multiple orders of magnitude larger. Thus one can assume that the deviations are more likely caused by the simulation itself than by the different setups and roughly describe the accuracy with which the d80, r_{det} and d_{min} can be measured.

4.2 Displacing two cameras symmetrically

Next two cameras were moved at the same time in a way that the setup could remain symmetrical. The results were analyzed to find out whether or not the reference setup can be improved by using different camera positions. Therefore separate shifts in x-, y- and z-direction of the global coordinate system were performed for the cameras.

The first changes were made in x-direction. For this purpose, the distance between the cameras within one camera row was changed while the other cameras remained in their positions. Initially only the positions of the cameras were changed while their orientations stayed the same. This led to the mirror moving out of the field of view of the shifted cameras after a certain distance had been surpassed. A strong increase of the d80 could be observed for those images (see figures 12 and 13). The d80 almost doubles for the lower camera row and the increase of the upper camera row is almost as large.
After that the simulations for the images with a clipped mirror coverage were repeated, but this time the cameras were realigned, so that the whole mirror surface was covered at all times. As seen in figures 12 and 13, the d80 stays within a range of 5 percent now, with deviations of up to 3.93 percent after displacing the upper and 3.70 percent after displacing the lower row.

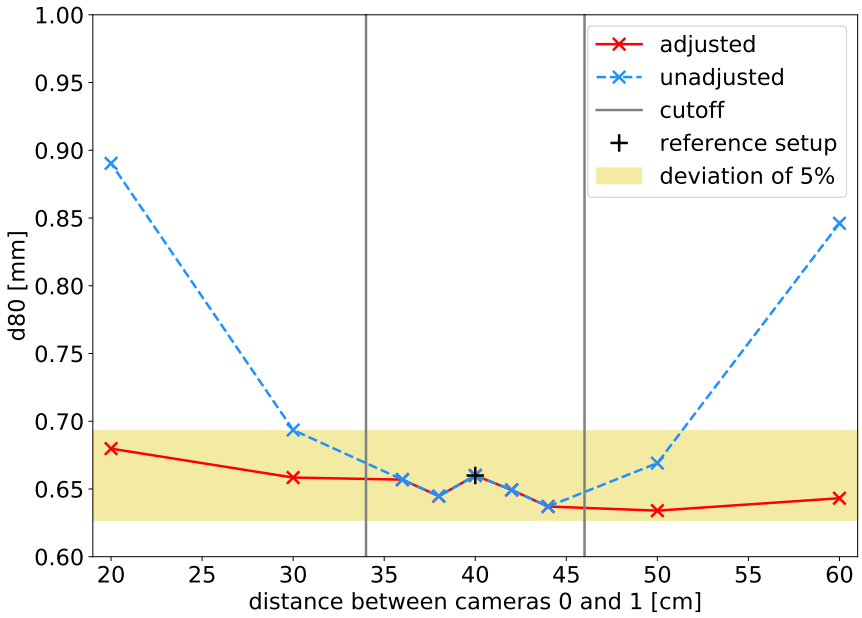

Figure 12: d80 as a function of the distance between camera 0 and 1 in x-direction. Compared are simulations with adjusted camera orientations to guarantee the full coverage of the mirror by the cameras and the unadjusted simulations that clip parts of the mirror after a certain distance.

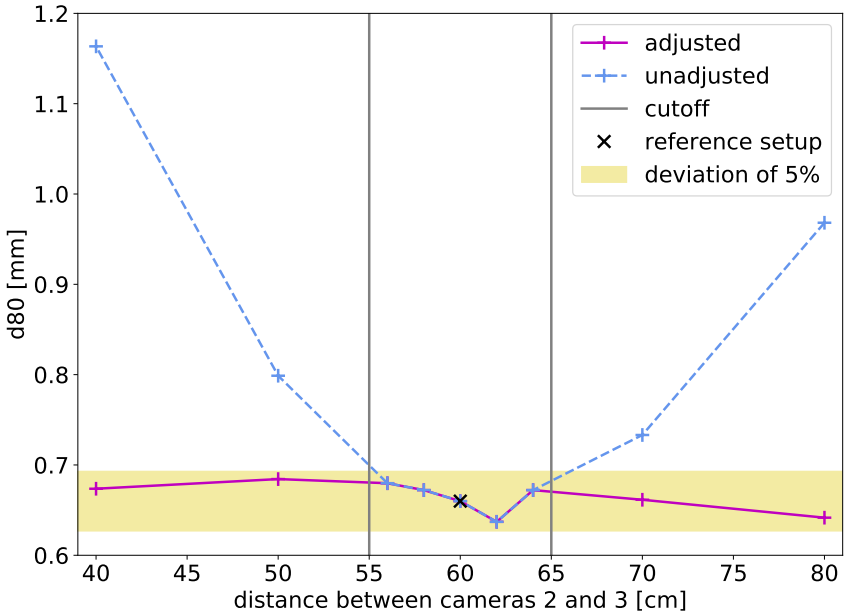

Figure 13: d80 as a function of the distance between camera 2 and 3 in x-direction. Compared are simulations with adjusted camera orientations to guarantee the full coverage of the mirror by the cameras and the unadjusted simulations that clip parts of the mirror after a certain distance.

Partially moving the mirror out of the field of view of the cameras leads to a loss of data which influences the results. As seen in figure 14, the PSF takes on a slightly elliptical shape resulting in a more widespread intensity distribution which causes the d80 to widen.
Additionally, it is noticeable that the deviations of the clipped simulations reach slightly bigger values when the lower camera row is shifted instead of the upper camera row. One possible explanation could be the sight angle of the cameras relative to the mirror surface. Since camera 2 and 3 are placed lower in the setup, they have a flatter angle of incidence with respect to the mirror than camera 0 and 1. This leads to a more distorted view of the screen and could potentially cause bigger deviations.

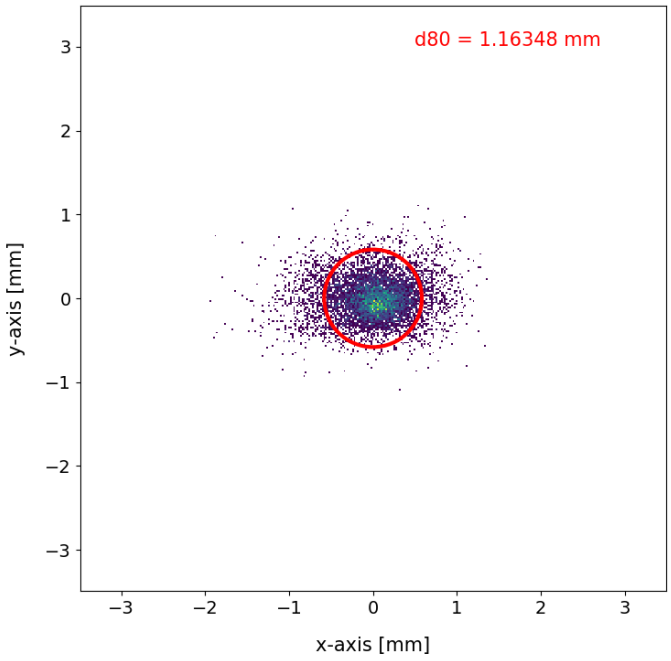

Figure 14: PSF and d80 for the simulation in which the distance between camera 2 and 3 in x-direction equals 40 cm.

Changes regarding the y-coordinates of the two camera rows have been made in the next simulation series. The upper and lower camera rows were shifted separately in positive and negative y-direction to assure a symmetrical setting. First cameras 0 and 1 were shifted while cameras 2 and 3 stayed fixed, then cameras 2 and 3 were shifted while cameras 0 and 1 maintained their position. In this case, the entire mirror surface was observed at all times from the beginning, so that no data would be lost.
While no boundaries were found for the simulated displacements in x-direction, there are boundaries for changing the y-coordinates of the cameras. If the camera rows were moved too much, the screen pattern moved out of the field of view of the cameras. This would lead to the same result as clipping a part of the mirror, which is losing data, and this loss would initiate an increase of the d80 once again. Increasing the distance between the two camera rows by moving the upper row in y-direction led to a loss of data after 5 mm. The lower row could in total be positioned 12 cm away from the upper row without losing data. Moving the rows until they reached the same y-coordinates did not have any negative influence on the coverage. Tests with the lower camera row closer to the mirror than the upper row were not performed since this would change the schematics of the setup and would not correspond to the model construction.
If full coverage of the mirror surface is ensured, then the results do not differ much from the reference values, similar to the displacement in x-direction. Compared to the reference setup, the d80 stays within a 2.31 percent range after displacing the upper and a 4.16 percent range after displacing the lower camera row. The results for the d80 after changing the y-coordinates of the cameras can be found in the appendix (see tables 8 and 9).

Lastly, the process was repeated for the distance between the camera rows in z-direction. The displacement of the upper and lower camera row was once again performed individually. Like in y-direction, boundaries could be found regarding the placement of the cameras. In general only camera positions were examined where the distance between the camera rows could remain at least 10 cm, so that the design still maintained a sufficient similarity to the model. This resulted in the upper cameras having only one upper boundary that is located 7 mm above the reference position. The only boundary for the lower cameras is 4.9 cm below their reference position. The results for the d80 at different camera positions in z-direction resemble the ones for changes in x- and y-direction as long as the mirror coverage is ensured. After displacing the lower row, the d80 reaches deviations of up to 5.08 percent from its reference value and 2.08 percent after shifts of the upper row. All values can be found in tables 10 and 11 in the appendix.

The values for r_{det} and d_{min} in the simulations with two symmetrical displaced cameras in x-, y- and z-direction and realigned camera orientations remain relatively constant again, reaching deviations of up to 0.03 percent to the reference values. Unlike for the d80, the cut-off of the mirror surface from the field of view of the camera does barely influence the r_{det} and d_{min}. The deviations from the reference setup remain below 0.08 percent which is still in the same order of magnitude as the values measured for the realigned camera positions.
Since shifting two cameras symmetrically in any direction does neither improve nor worsen the d80 heavily as long as a full coverage of the mirror can be guaranteed, multiple equally good implementations for the positions and orientations of the cameras within the aforementioned spatial boundaries are possible.

4.3 Testing different camera and screen resolutions

Next tests concerning the resolutions of the cameras and screen were performed. For that two series of simulations were conducted. For the first series, the reference screen resolution of 1920×1080 (HD) was maintained while different camera resolutions were tested. Later the resolution of the screen was raised to 3840×2160 (4K) and the simulation was repeated for varying camera resolutions. The size of the screen and the CCD-chips stayed the same throughout both series. The results can be seen in figure 15.
Decreasing the camera resolution leads to the same results for both screen resolutions. The d80 increases quickly, even reaching a value that is 5.7 times higher when compared to the reference d80. But if the camera resolution is increased, the results show differences for the two simulations. While the d80 of the simulation with HD screen resolution remains approximately constant, staying roughly in a 5 percent range after reaching the reference camera resolution, the d80 of the simulation with a 4K screen continues to decline noticeably albeit slower. After reaching a camera resolution that is four times as good as the reference one, the d80 is almost half as large as the one with the HD screen resolution.

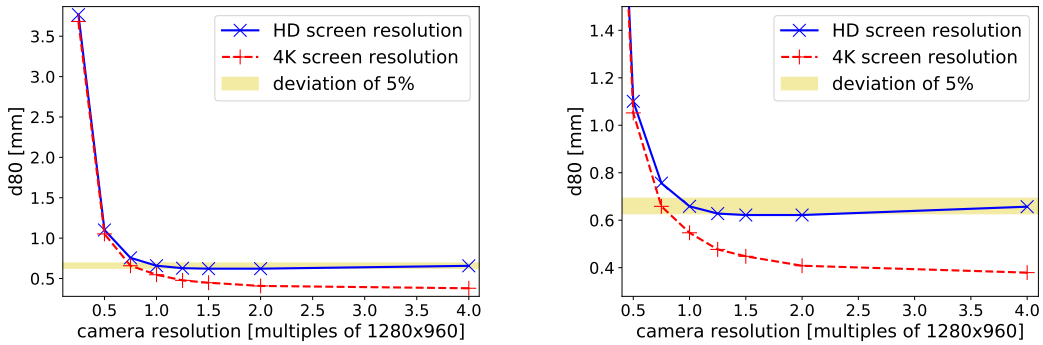

Figure 15: d80 as a function of the camera resolution with a zoom-in for the range between 0.5 and 4 times the camera resolution on the right side. Compared are the results for a HD and 4K screen resolution. Deviations from the reference value within a range of 5 percent are marked in yellow.

Since each pixel of the screen acts as a light source in the setup, edge effects must be taken into account that lead to an additional expansion of the PSF. The larger the pixels are, the more influence the edge effects have on the calculation of the PSF and thus also on the d80. Because the resolution of the HD screen is worse than that of the 4K screen, the pixel size of the HD screen is consequently larger. Therefore edge effects have more influence and the PSF of the HD screen simulations extends slightly more which generally leads to a higher d80 in comparison to the results of the 4K resolution.
However, in order to take advantage of the high screen resolution, a camera with a sufficiently high resolution is also necessary. If the camera resolution is below a certain value, the images taken by it cannot be distinguished from each other despite the different screen resolutions. This leads to similar results after the evaluation of the aforementioned images. As can be seen in figure 15, the d80 of the HD and 4K simulations does not differ much for camera resolutions below 0.75 times the reference resolution (960×720). This marks the lower limit at which the cameras can discern the different screen resolutions in the table-top setup.
At the same time the camera resolution does not have to be infinitely high, as one can see in figure 15. Above a certain value in the upper camera resolution range, the test results are limited by the screen resolution which means having very high resolution cameras would be unnecessary. While they could not accomplish better results, the costs for those cameras would be higher.
If the aforementioned facts concerning the combination of screen and camera resolutions are taken into account, an improvement of the cameras would not be necessary for the reference setup. However, if a 4K screen is used in the future setup, it would be worthwhile to work with a camera resolution that is twice as good as the one used in the reference setup as it would achieve the best results for the lowest possible price of the cameras.
The r_{det} and d_{min} are apparently not dependent on different sets of camera and screen resolutions. They differ from the reference values no more than 0.05 percent and do not show a distinctive behavior.

5 Alterations of the table-top setup due to external influences

In the previous chapter, the general behavior of the newly designed table-top setup was studied. The exact spatial and intrinsic parameters of all needed objects were known at all times. In the case of a simulation, this can always be ensured. However, it is not always achievable to know these parameters for the real table-top setup. Unintentional changes can be caused by external influences, such as impacts on the setup or the temperature dependence of the materials, after the setup has been calibrated. This could impact the results negatively.
In the following chapter, it will be examined to what extent unintentional changes can influence the measurement. For this purpose, the effect of shifting and tilting camera 0 after the setup has been calibrated is studied. For that, camera 0 is displaced and misaligned in the simulation while the reference setup layout is used for the analysis to imitate disruptions caused by external influences

5.1 Tilting camera 0

The position and orientation of camera 0 in the simulation is determined by its position and direction vector in the global coordinate system. While the zerobase of camera 0 determines its spatial coordinates, the xbase and ybase determine the orientation of the camera in the global coordinate system. The ybase also defines the direction of the camera view. xbase, ybase and the vector perpendicular to them, the zbase, additionally form the base vectors of the coordinate system of the camera.
In the following, camera 0 was only tilted while its position remained the same. In order to change the orientation of the camera, the parameters for the ybase, i.e. the viewing direction, of the camera were altered. The ybase of the camera was tilted at a certain angle in positive and negative directions of the base vectors of the coordinate system of the camera, i.e. the xbase and the zbase. As seen in figure 16, the d80 increases quickly with a growing inclination from the nominal direction for angular changes in the order of 0.001 degree. A deviation of 29.43 percent from the reference value can even be observed for an inclination of 0.005 degree in negative x-direction.

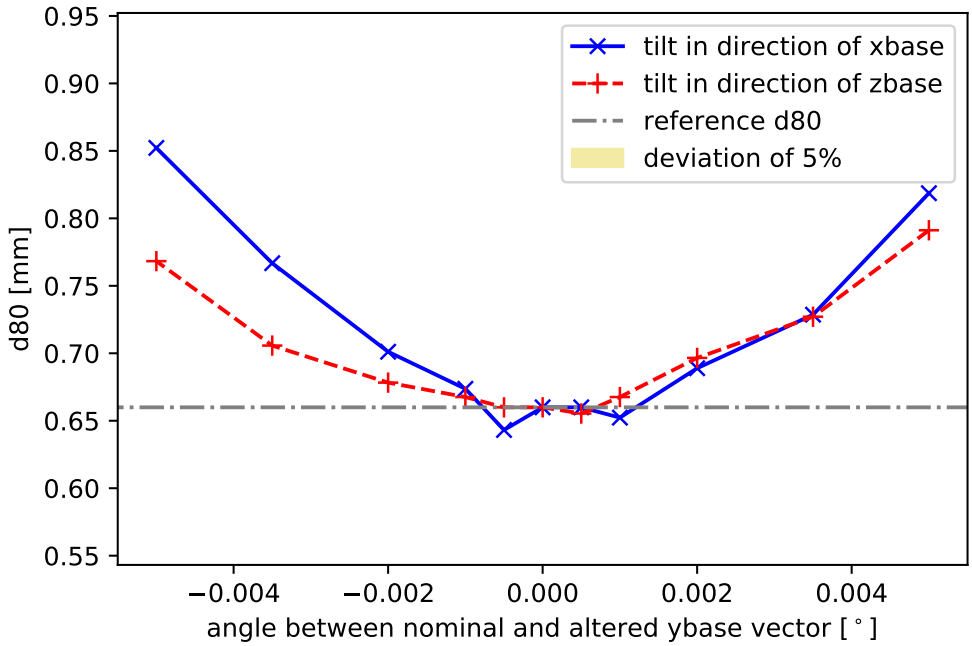

Figure 16: d80 as a function of the angular mismatch between the nominal and altered direction vector of camera 0 for inclinations in direction of the xbase and zbase of the camera. Deviations from the nominal value within a range of 5 percent are marked in yellow.

In the following section, the distance between the intersection point of the nominal direction vector of camera 0 with the screen and that of the altered direction vector with the screen was calculated in units of screen pixels under the assumption that the mirror is planar. This simplified model was calculated to get an estimate on how many screen pixels correspond to the misalignment of the camera.
Since the position and orientation of camera 0 and the screen are known and the mirror is assumed to be planar, the intersection of the direction vector of the camera with the screen can be calculated by mirroring the screen on the x-y-plane of the global coordinate system (see figure 17).

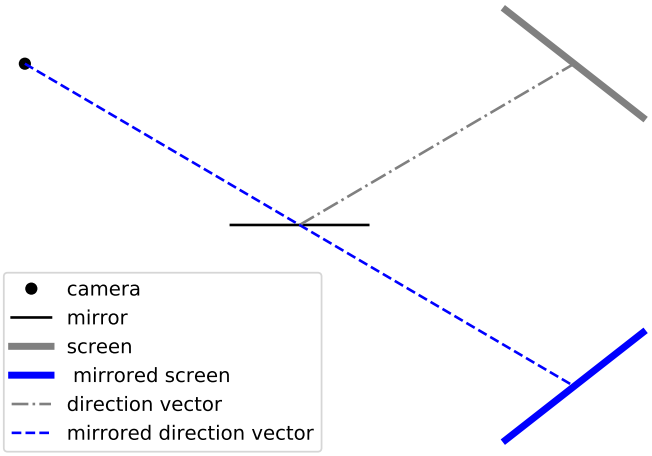

Figure 17: Schematics to calculate the intersection of the direction vector of camera 0 with the screen.

For that, one has to find the linear equation for the direction vector of camera 0 (1) and the plane equation for the screen (2) and then solve the following system of equations (3):

$$\vec{S}_{\text{intersect}} = \overrightarrow{zerobase}_{\text{cam}} + \overrightarrow{ybase}_{\text{cam}} \cdot q \tag{1}$$

$$\vec{S}_{\text{intersect}} = \overrightarrow{zerobase}_{\text{screen}} + \overrightarrow{xbase}_{\text{screen}} \cdot s + \overrightarrow{ybase}_{\text{screen}} \cdot r \tag{2}$$

$$\overrightarrow{zerobase}_{\text{cam}} + \overrightarrow{ybase}_{\text{cam}} \cdot q = \overrightarrow{zerobase}_{\text{screen}} + \overrightarrow{xbase}_{\text{screen}} \cdot s + \overrightarrow{ybase}_{\text{screen}} \cdot r \tag{3}$$

Then the scalars s and r are inserted back into (2) and the intersection point can be calculated. Afterwards the distances $d_{\text{x, screen}}$ and $d_{\text{y, screen}}$ of the intersections can be calculated for x- and y-coordinates in the coordinate system of the screen:

$$d_{\text{x, screen}} = x_{\text{S, alt}} - x_{\text{S, nom}}$$

$$d_{\text{y, screen}} = \pm \sqrt{(y_{\text{S, alt}} - y_{\text{S, nom}})^2 + (z_{\text{S, alt}} - z_{\text{S, nom}})^2}$$

Since the x-direction of the global coordinate system matches the x-direction of the screen coordinate system, the distance in x-direction is calculated by simply subtracting the nominal intersection value from the altered one. In order to get the distance in units of screen pixels, one has to divide the results for $d_{\text{x, screen}}$ and $d_{\text{y, screen}}$ by the pixel size of the screen which equals 312.5 µm. Table 4 shows the results of the calculations for the distances between the geometric intersection points. In the nominal setup the direction vector of camera 0 is aligned close towards the center of the mirror. Table 4 shows that the distance between the nominal and the new intersection points is smaller than the size of one screen pixel for all performed misalignments.

angular change [°]	$d_{\text{x, screen}}$ for tilt in x [# pixels]	$d_{\text{y, screen}}$ for tilt in x [# pixels]	$d_{\text{x, screen}}$ for tilt in z [# pixels]	$d_{\text{y, screen}}$ for tilt in z [# pixels]
0.005	0.35	0	-0.07	-0.46
0.0035	0.24	0	-0.05	-0.33
0.002	0.14	0	-0.03	-0.19
0.001	0.07	0	-0.01	-0.09
0.0005	0.03	0	-0.01	-0.05
-0.0005	-0.03	0	0.01	0.05
-0.001	-0.07	0	0.01	0.09
-0.002	-0.14	0	0.03	0.19
-0.0035	-0.24	0	0.05	0.33
-0.005	-0.35	0	0.07	0.46

Table 4: Distances between the nominal and altered intersection points of the screen and camera perspective in units of screen pixels depending on the angular changes. The results were rounded to two decimal places.

Another way to get information about the size of the pixel shift caused by angular change is to directly read out the information from the results of the PMD measurements. This has to be done for each camera pixel individually. One chooses a certain camera pixel and reads out the coordinates of the screen pixel that are mapped to that camera pixel for all angular changes. Now the resulting coordinates of the nominal and altered camera settings can be directly subtracted from each other since they are already defined in terms of the screen coordinate system. In the following, this was performed using camera pixel (650,500), a pixel that is relatively close to the center of the mirror, as an example (see table 5). The size of one camera pixel equals 3.75 µm.
The second method gives similar results to the previous geometric solution. The pixel shift that corresponds to angular changes, such as the ones performed in this simulation, is still smaller than the size of one screen pixel. But unlike in the geometric method, the results for positive and negative inclinations are not as symmetrical. Since the distances which correspond to the misalignments of camera 0 were created by reading out information of the PMD program in the second method, it can be assumed that the symmetry errors, which are only in the range of 0.03 pixel sizes, are probably numerical errors.

angular change [°]	$d_{\text{x, screen}}$ for tilt in x [# pixels]	$d_{\text{y, screen}}$ for tilt in x [# pixels]	$d_{\text{x, screen}}$ for tilt in z [# pixels]	$d_{\text{y, screen}}$ for tilt in z [# pixels]
0.005	0.34	0	-0.07	-0.47
0.0035	0.25	-0.01	-0.04	-0.35
0.002	0.14	-0.01	-0.02	-0.20
0.001	0.07	-0.02	-0.01	-0.10
0.0005	0.04	-0.02	-0.01	-0.06
-0.0005	-0.03	-0.03	0	0.02
-0.001	-0.07	-0	0.02	0.09
-0.002	-0.13	-0.02	0.03	0.17
-0.0035	-0.24	-0.01	0.05	0.32
-0.005	-0.34	-0.02	0.08	0.45

Table 5: Distances between the nominal and new screen pixel coordinates that are mapped to the camera pixel (650,500) in units of the screen pixels after tilting camera 0. The results were rounded to two decimal places.

Figure 16 shows that the d80 increases visibly after misalignments in the order of 0.001 degree even though the corresponding pixel shift is smaller than the size of one screen pixel. If one assumes that a camera pixel is mapped to the center of a screen pixel, a shift the size of the ones seen in the previous tables 4 and 5 would not result in a pixel offset after misalignments of camera 0. But because the pixel size of the camera does not equal the one of the screen, multiple camera pixels cannot be centered in the middle of a screen pixel. Some of them are mapped close to or even on top of a border between two screen pixels. In that case, misalignments that correspond to pixel shifts smaller than the size of one screen pixel could also lead to a pixel offset. The stronger the misalignments are, the more camera pixels observe screen pixels different to the ones observed in the reference setup which results in an increasing d80.
In addition to that, edge effects could possibly influence the measurement since the camera is not directed perpendicular to the screen and the mirror is actually not planar. As a result, the distance between the nominal and altered intersection points correspond to a slightly different pixel shift for each individual camera pixel. Camera pixels that depict the edge of the mirror could generally have a different pixel offset than ones that are located more towards the center of the mirror. This spatial dependence might be powerful enough to increase the d80 even further.

5.2 Changing the position of camera 0

The last series of simulations include shifting camera 0 out of its nominal position without changing the angle at which the direction vector of the camera hits the screen. For that, translations of camera 0 in x-, y- and z-direction of the camera coordinate system were performed individually. The results for the d80 can be seen in figures 18 and 19.

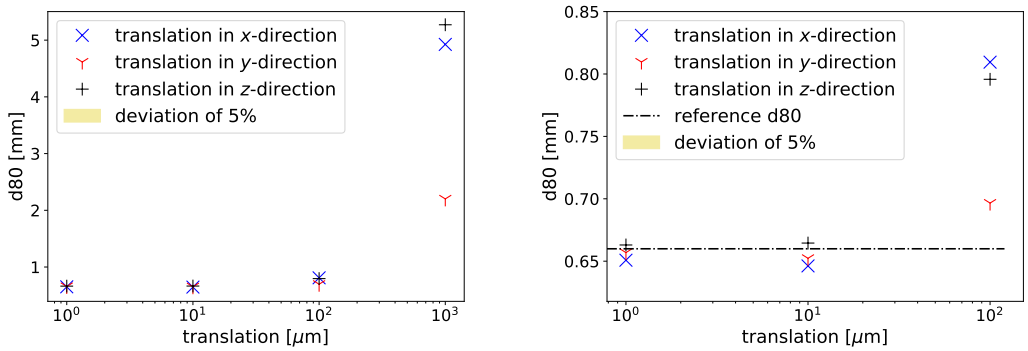

Figure 18: d80 after a translation in positive x-, y- and z-direction of camera 0 with a zoom-in for the range between $10^0\,\mu$m and $10^2\,\mu$m on the right side.

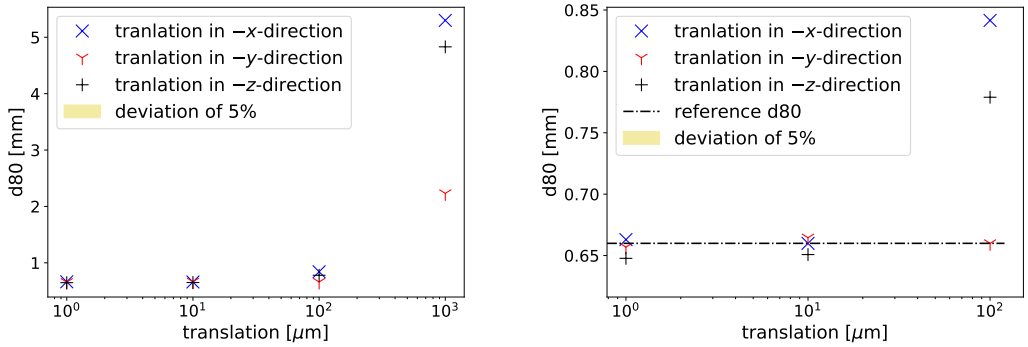

Figure 19: d80 after a translation in negative x-, y- and z-direction of camera 0 with a zoom-in for the range between $10^0\,\mu$m and $10^2\,\mu$m on the right side.

The d80 rises quickly for increasing offsets in every direction. While displacements of 100 µm can already reach deviations to the reference d80 of up to almost 30 percent, displacements of 1 mm cause values more than seven times higher than the reference (see translations in negative x-direction). The translation in y-direction affects the d80 the least. The reason for that is that a translation along the y-axis of the camera coordinate system does actually not change the view of the camera because the direction vector of the camera is defined by its ybase vector, which in turn defines the y-axis of the camera coordinate system. The translations along the x- and z-axis change the view of camera 0. This results in a higher rise of the d80 in comparison to the y-direction alterations, as can be seen in figures 18 and 19.

Like in section 5.1, the distance between the intersection point of the nominal and the altered direction vector and the screen was calculated afterwards. The calculation itself can be carried out as for the simulations with angular changes. Again, a planar mirror is assumed and the screen is mirrored on the x-y-plane of the global coordinate system to simplify the calculations. The results can be seen in table 6.

shift [µm]	$d_{\text{x, screen}}$ for shift in x [# pixels]	$d_{\text{y, screen}}$ for shift in x [# pixels]	$d_{\text{x, screen}}$ for shift in z [# pixels]	$d_{\text{y, screen}}$ for shift in z [# pixels]
1000	3.28	0	-0.68	-4.39
100	0.33	0	-0.07	-0.44
10	0.03	0	-0.01	-0.04
1	0	0	0	0
-1	-0	0	0	0
-10	-0.03	0	0.01	0.04
-100	-0.33	0	0.07	0.44
-1000	-3.28	0	0.68	4.39

Table 6: Distances between the nominal and altered intersection points of the screen and the direction vector of camera 0 in units of screen pixels depending on its translation in x- or z- direction. The results were rounded to two decimal places.

The calculations for the y-shift are not included in the table above because the y-direction of the camera equals its perspective vector. Shifts in this direction do not lead to a different intersection point with the screen. If calculated, the results for y-shifts would be consistently 0.
Translations with the size of 1 mm finally lead to distances between the intersection points corresponding to more than the size of one screen pixel.

The method, in which the distance between the nominal and altered screen pixels observed by camera pixel (650,500) is calculated, was also repeated. The results can be seen in table 7.

shift [µm]	$d_{\text{x, screen}}$ for shift in x [# pixels]	$d_{\text{y, screen}}$ for shift in x [# pixels]	$d_{\text{x, screen}}$ for shift in y [# pixels]	$d_{\text{y, screen}}$ for shift in y [# pixels]	$d_{\text{x, screen}}$ for shift in z [# pixels]	$d_{\text{y, screen}}$ for shift in z [# pixels]
1000	3.21	0	0	-0.02	-0.70	-4.31
100	0.33	-0.01	-0.01	-0.01	-0.07	-0.46
10	0.05	-0.02	0.01	-0.01	-0.01	-0.06
1	0.01	0	0.01	-0.01	0	-0.01
-1	0	-0.02	0	-0.02	0.01	0.01
-10	-0.03	-0.03	0	0	0	0.04
-100	-0.31	-0.01	0	0	0.08	0.43
-1000	-3.23	-0.02	0.01	0.01	0.67	4.29

Table 7: Distances between the nominal and new screen pixel coordinates that are mapped to the camera pixel (650,500) in units of the screen pixels depending on its translation in x-, y- or z-direction. The results were rounded to two decimal places.

Again, the results for the distances $d_{\mathrm{x,\,screen}}$ and $d_{\mathrm{y,\,screen}}$ resemble the ones calculated with the geometric method. If the camera is translated 1 mm in x- or z-direction, the distance between the nominal and new screen pixel that is mapped to camera pixel (650,500) is larger than the size of a screen pixel. The other translations that were performed resulted in shifts below the size of a screen pixel. The results of the second method show an asymmetry just like for misalignments of the camera, especially for shifts in y-direction where no pixel offset should be measured since the same screen pixels are still observed before and after the translation. These symmetry deviations lie in the same range as for the simulation with the misaligned camera, so it can be assumed that they are also caused by numerical errors.

In general, one can differentiate between simulations in which the translation of camera 0 is below the pixel size of one screen pixel and simulations in which the translation is above this pixel size. By the simplified assumption that the examined mirror is planar, the angle of incidence of the camera to the screen is not changed. Thus the shift of the camera in x-direction corresponds to the x-shift on the screen. A shift in x-direction by a multiple of 312.5 µm corresponds to roughly the multiple of a screen pixel, which matches the results of the 1 mm translation in x-direction. Every camera pixel will observe a pixel offset if the camera is shifted more than the size of a screen pixel. This results in a very strong increase of the d80.
Translations of the camera that do not automatically lead to a pixel shift lie roughly below the size of a screen pixel. But in figures 18 and 19 one can see that the d80 is also noticeably increased for translations of 100 µm. Similar to the simulation with changed alignments, this may be due to the fact that enough camera pixels, which are not projected into the center of a screen pixel, observe a pixel offset by viewing screen pixels that differ from the ones observed in the reference setup. This would result in an increase of the d80.
The additional increase of the d80 due to potential edge effects cannot be completely rejected, as shifts for camera pixels at the edge of the mirror correspond to slightly different pixel shifts than ones for camera pixels in the center of the mirror. In order to find out how much influence this spatial dependency really has, further investigations have to be undertaken.

Taking the results concerning the misalignment and disposition of camera 0 into consideration, it seems like the post-calibration of the spatial camera parameters, which is performed automatically in each sphere-fit evaluation, is not capable of calibrating small disruptions such as the ones performed in this thesis. Therefore it is important for the setup which is about to be built that one pays great attention to shield it as well as possible from external influences that could displace or misalign parts of the setup after the calibration.

6 Summary and outlook

The goal of this thesis was to design a table-top setup for a Phase Measuring Deflectometry station and to study the sensibility of this designed table-top layout. Since the PMD method is already commonly used to measure reflective surfaces, including CTA mirror facets, the table-top design should help to further investigate the systematics of the PMD measurement technique. Thereby no ongoing measurements performed on the setup designed to measure the aforementioned mirrors have to be interrupted or delayed.

First, a short introduction about gamma-ray astronomy and the CTA project, which is intended to become one of the leading research projects in the field of astroparticle physics, was given. Then the PMD method and the existing PMD mirror measuring setup for the current CTA mirrors were presented. For this purpose, four cameras to completely cover the surveyed mirror and a screen, that projects a pattern of two coprime sinusoidal intensity distributions, were needed. Since the table-top setup was simulated, the basics of ray-tracing were shortly explained afterwards.
Then the derived properties of the table-top setup were presented. This included the positions and orientations of the objects used in the setup and the results for the PMD and PSF measurements, meaning the d80, the determined radius of curvature of the mirror and the distance from the mirror at minimal d80 for the $2f$ ray-tracing. These values served as references for all of the following simulations. Then different parameters of the setup were altered and it was examined whether they had a positive or negative effect on the test results. In the beginning, cameras 0 and 3 were displaced separately in x-direction of the global coordinate system. This resulted in d80 values that deviated in a range of 2.08 percent from the reference value after displacements of camera 0 and 3.47 percent after displacements of camera 3. It was also discovered that the determined radius of curvature and distance with minimal d80 did not change much even though the d80 fluctuated slightly. In general, none of the deviations showed a distinctive pattern after the displacements. Afterwards, two cameras were shifted symmetrically. This led to deviations in the same order of magnitude as for shifting one camera as long as a full coverage of the mirror was guaranteed. Additionally, boundaries for the positioning of the cameras were identified for the y- and z-direction. Different sets of camera and screen resolutions were also tested. It was shown that the camera resolution of the reference setup is sufficient when using a HD screen and that a resolution that is twice as good as the reference one would be optimal for the 4K screen resolution.
Lastly, camera 0 was displaced and misaligned in the simulation while the reference setup layout was used for the analysis to imitate disruptions caused by external influences. It was discovered that minor alterations within the setup can cause a high increase of the d80, even reaching values more than seven times higher than the reference value after displacing the camera only 1 mm. The distances in units of screen pixels that corresponded to the performed displacements and misalignments were calculated geometrically and also read out from the PMD

program. The alterations of camera 0 did not cause a pixel shift the size of a whole screen pixel for all modifications except for displacements of 1 mm. There it corresponded to an offset of three pixels in x-direction of the screen, after a translation of the camera in x-direction in the camera coordinate system, and four pixels in y-direction of the screen, after a translation in z-direction in the camera coordinate system.

Through the work done in this thesis, it was shown that the derived layout for a table-top PMD station does work and can be used in the future to further analyze the PMD measurement technique. Therefore one can now begin to construct the setup. Since the spatial restrictions for the measurement setup, which ensure full coverage of the mirror, could already be found with the help of the simulations, one can begin to build the mounting bracket for the four cameras and the screen. Due to the study of disruptions caused by external influences, it is known that already small incorrect configurations, such as displacements of a camera in the order of a few 100 µm or misalignments in the order of 0.001 degree, can have greater effects on the test results. This has to be taken into account when building the fixture. A robust mount should be chosen and contact with the measurement setup should be avoided as much as possible after it has been calibrated. Possible first measurements after the construction can then include the recreation of the measurements simulated in this thesis in order to find out to what extent the obtained results differ from the simulations.

Appendix

distance between upper and lower camera row in y-direction [cm]	d80 [mm]
5	0.65994
4	0.65842
3	0.66605
2	0.66299
1	0.67520
0	0.65842

Table 8: d80 at varying distances between the upper and the lower camera row after shifting the upper row in y-direction.

distance between upper and lower camera row in y-direction [cm]	d80 [mm]
10	0.68741
7	0.65689
6	0.65231
5	0.65994
4	0.65994
3	0.64774
2	0.63553
1	0.63095
0	0.63553

Table 9: d80 at varying distances between the upper and the lower camera row after shifting the lower row in y-direction.

distance between upper and lower camera row in z-direction [cm]	d80 [mm]
20.5	0.64776
20	0.65994
19.5	0.65079
19	0.64621
18	0.65079
15	0.65842
10	0.67368

Table 10: d80 at varying distances between the upper and the lower camera row after shifting the upper row in z-direction.

distance between upper and lower camera row in z-direction [cm]	d80 [mm]
22	0.68130
21	0.67062
20.5	0.66605
20	0.65994
19.5	0.65994
19	0.65384
18	0.65384
15	0.62790
10	0.62637

Table 11: d80 at varying distances between the upper and the lower camera row after shifting the lower row in z-direction.

References

[1] Acharya, B.S., Actis, M., Aghajani, T., et al.: Astroparticle Physics, 43 (2013), 3-18

[2] Actis, M., Agnetta, G., Aharonian, F., et al.: Experimental Astronomy, 32 (2011), 193-316

[3] Cern (2018): Cosmic rays: particles from outer space, `https://home.cern/science/physics/cosmic-rays-particles-outer-space` [27.12.2018]

[4] CTA (2016): How CTA detects Cherenkov light, `https://www.cta-observatory.org/about/how-cta-works/` [29.12.18]

[5] CTA (2016): The technology behind the next generation very-high energy gamma-ray detector, `https://www.cta-observatory.org/project/technology/` [29.12.18]

[6] Pickel, Stefan (2014): Simulation of a setup for phase measuring deflectometry

[7] Specovius, Andreas (2016): Measurement of aspherical mirrors with PMD

[8] Wenzel, Jakob (2010): Mitsuba Physically Based Renderer, `http://mitsuba-renderer.org/` [25.01.19]

[9] Wörnlein, André (2012): Methods to measure optical properties of mirror facets for CTA

Danksagung

Zum Schluss möchte ich mich noch bei allen bedanken, die zum Gelingen dieser Arbeit beigetragen haben. Insbesondere möchte ich mich bedanken bei:

- Prof. Dr. Christopher van Eldik für die Vergabe des spannenden Themas und die Betreuung der Arbeit.
- Andreas Specovius für die großartige Unterstützung, ein stets offenes Ohr für all meine Fragen und das Korrekturlesen.
- Johannes Veh, Franziska Eberle und Michael Zeiler für das Korrekturlesen und ihre hilfreichen Verbesserungsvorschläge.
- Der gesamten Arbeitsgruppe für die herzliche Aufnahme und das Verschaffen einer angenehmen Arbeitsatmosphäre.
- Meinen Eltern und meinem Bruder Max für die Unterstützung während meines gesamten Studiums.

Erklärung

Hiermit bestätige ich, dass ich diese Arbeit selbstständig und nur unter Verwendung der angegebenen Hilfsmittel angefertigt habe.

Erlangen, den 30. 01. 2019

Franziska Leitl